

A NEW VIEW OF TYCHO AND COPERNICUS CRATERS' SECONDARY CRATER POPULATIONS.

K. S. Wells¹, D. B. Campbell¹, B. A. Campbell², L. M. Carter³, ¹Cornell University, 514 Space Sciences Building, Ithaca, NY 14853, ²Smithsonian Institution, ³NASA Goddard Space Flight Center; kassiew@astro.cornell.edu; campbell@astro.cornell.edu.

Introduction: To refine crater-derived ages throughout the Solar System, the relative abundance of primary and secondary craters on the Moon must be understood. The secondary crater populations of large, young lunar primary craters like Copernicus ($D = 93$ km) and Tycho ($D = 95$ km) are ideal testing grounds because they are the best-preserved examples of large secondary crater networks. We investigate the abundance and distribution of Copernicus and Tycho secondary craters using 2.38 GHz (13-cm) Arecibo-Green Bank Telescope radar circular polarization ratio (CPR) mosaics. Radar CPR is the ratio of the signal received in the same polarization sense as transmitted to the signal received in the opposite sense as transmitted. A specular surface has a CPR of zero, with rougher surfaces at higher values, making radar CPR a good indicator of surface roughness.

One of the difficulties in identifying secondary craters is that their most obvious morphological characteristics—elliptical planforms, shallow floors, herringbone formations, etc.—are most pronounced near the parent crater, where secondary craters are formed from relatively low-velocity ejecta. Higher impact velocities make these characteristics more subdued, complicating identification of secondary craters further from the parent crater. However, the down-trajectory momentum component of secondary-forming ejecta fragments is higher for higher velocity ejecta. Workers have hypothesized that this creates a surge of downrange secondary ejecta and local materials.¹ This hypothesis is supported by the presence of streaks of increased roughness down-range from secondary craters in Copernicus rays (Figure 1). These streaks of increased

roughness are also seen around obvious Tycho secondary craters, and can be used as a proxy for identifying new secondary craters that are not obvious candidates based on their morphology. For more information on this method, see Wells et al. (2010), who use radar CPR to identify Tycho secondary craters near the lunar South Pole.²

Discussion: Using the method described above, we identify large numbers of Copernicus and Tycho secondary craters ranging in distance from 1-10 crater-radii from the parent impact. Understanding how the number of secondary craters produced changes as a function of distance from the parent crater will help us predict the total number of secondaries associated with a given impact. To address this issue, we compute secondary density as a function of range from the parent crater. Density is defined here as $N(1)$, the number density of secondary craters with diameters greater than or equal to 1 km. For Copernicus crater, $N(1)$ was computed by azimuthally averaging all craters identified and dividing the population into radial bins of width 46.5 km (the Copernicus crater radius). The $N(1)$ values shown in Figure 2 suggest that the azimuthally-averaged density of secondary craters remains non-negligible for large distances, falling below $N(1)=0.001$ (equivalent to an ~ 1 Gyr primary population)³ only beyond seven crater radii.

We also infer ejecta fragment size and the distribution of kinetic energy in the ejection process. Our results match well with Vickery (1987), who calculated the maximum size of Copernicus ejecta fragments as a function of range.⁴ Impact velocity is computed based on distance from the parent crater. Ejecta fragment

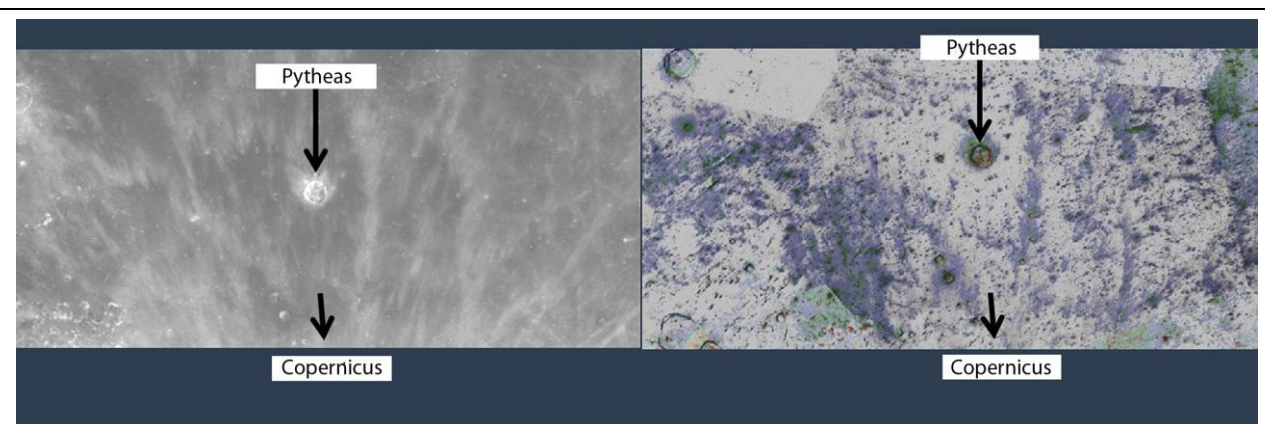


Figure 1. A comparison between a Clementine 750 nm image of Copernicus rays (left) and a radar CPR mosaic of the same region (right). Areas with high-CPR values are overlaid in red, blue, and green on an 80 m/pix radar depolarized map. These areas have enhanced roughness on the 13-cm scale, compared to areas in grey. These rough streaks are oriented radially from Copernicus crater and correlate with the presence of rays in the Clementine image on the left. Note detailed structure is more apparent in the high-CPR image, aiding in the identification of secondary craters. Similar images were used to identify all secondary craters in this study.

size is inferred from crater size and impact velocity. Our results for the largest fragment at a given range are in good agreement with previous workers. Like Vickery (1987), we see an increase in fragment size for secondary craters closest to Copernicus. Vickery interpreted this not as an increase in actual fragment size for low-velocity ejecta, but as clusters of fragments forming a single crater. Our measurements of the fragment size-frequency distributions (SFDs) of Copernicus ejecta fragments also support this interpretation. The slope of the ejecta fragment SFDs, b_f , is typically estimated by the rule of thumb: $b_f \sim b/1.28$, where b is the secondary crater power-law slope. Since $b \sim -3$ to -4 for secondary crater populations, b_f values are typically between -2.5 and -3 .⁵ For regions near Copernicus, our measurements indicate somewhat steeper values ($b_f = -4.0$ or more), possibly as a result of additional comminution during flight in a very dense ejecta curtain. Values of b_f further from Copernicus were closer to $b_f = -3.0$, suggesting a thinning of the ejecta curtain with distance.

Summary: Our preliminary investigation of Copernicus and Tycho craters' secondary populations supports the interpretation that crater-forming impact ejecta significantly modifies the lunar surface for radial distances of hundreds of kilometers. For distances out to at least 10 crater radii, dense populations of Tycho and Copernicus secondary craters can be identified. They are associated with rough terrains that probably represent a mixture of primary and secondary ejecta as well as local materials whose down-range movement may have been initiated by the impact of secondary-crater forming material. The interplay of secondary crater formation and burial of pre-existing terrain by impact-related debris flow should be investigated in more detail, as both act to complicate chronologies derived from impact crater counts.

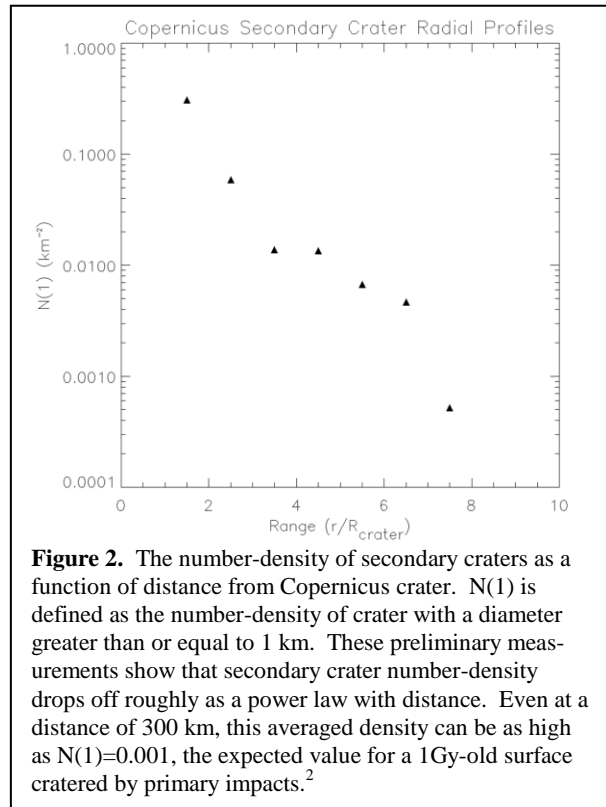


Figure 2. The number-density of secondary craters as a function of distance from Copernicus crater. $N(1)$ is defined as the number-density of crater with a diameter greater than or equal to 1 km. These preliminary measurements show that secondary crater number-density drops off roughly as a power law with distance. Even at a distance of 300 km, this averaged density can be as high as $N(1)=0.001$, the expected value for a 1Gy-old surface cratered by primary impacts.²

References: [1] Oberbeck, V.R. (1975), *Rev. Geophys. and Space Phys.*, 13, 337-362. [2] Wells, K. S. et al. (2010) *J. Geophys. Res.*, 115, E06008. [3] Neukum et al. (2001) *Space Sci. Rev.*, 96, 55-86. [4] Vickery (1987) *Geophys. Res. Letters*, 14, 726-729. [5] Hirata and Nakamura (2006), *J. Geophys. Res.*, 111, E03005.